

# Non-Negative Reduced Biquaternion Matrix Factorization with Applications in Color Face Recognition

Jifei Miao, Junjun Pan, and Michael K. Ng, *Senior Member, IEEE*

**Abstract**—Reduced biquaternion (RB), as a four-dimensional algebra highly suitable for representing color pixels, has recently garnered significant attention from numerous scholars. In this paper, for color image processing problems, we introduce a concept of the non-negative RB matrix and then use the multiplication properties of RB to propose a non-negative RB matrix factorization (NRBMF) model. The NRBMF model is introduced to address the challenge of reasonably establishing a non-negative quaternion matrix factorization model, which is primarily hindered by the multiplication properties of traditional quaternions. Furthermore, this paper transforms the problem of solving the NRBMF model into an RB alternating non-negative least squares (RB-ANNLS) problem. Then, by introducing a method to compute the gradient of the real function with RB matrix variables, we solve the RB-ANNLS optimization problem using the RB projected gradient algorithm and conduct a convergence analysis of the algorithm. Finally, we validate the effectiveness and superiority of the proposed NRBMF model in color face recognition.

**Index Terms**—Reduced biquaternion matrix, non-negative reduced biquaternion matrix factorization, reduced biquaternion projected gradient algorithm, color face recognition.

## I. INTRODUCTION

Numerous signal processing data exhibit nonnegativity, including images, material component quantities, word frequencies in documents, *etc.* To process these non-negative data, in 1999, Lee *et al.* introduced non-negative matrix factorization (NMF) [1], a technique that decomposes original data into two low-dimensional factor matrices: a basis matrix and an encoding coefficient matrix. Due to the implementation of non-negativity constraints, NMF results offer enhanced interpretability and a broad spectrum of practical applications [2], [3], as

each column of the basis matrix corresponds to a local feature while each column of the encoding coefficient matrix represents how a sample is expressed in a lower-dimensional space, allowing the original data to be interpreted as a purely additive combination of these basis features.

As a data analysis method, NMF has been proven to be useful in many real-world applications. In particular, its application in face recognition has been extensively studied [4]–[7]. Plentiful studies have shown that color information is beneficial for face recognition [8]–[12]. However, traditional NMF methods are inherently designed for grayscale face images. When performing color face recognition, NMF typically converts color images to grayscale or processes the three color channels of color face images independently [13], [14]. Both approaches lead to insufficient utilization of color information, resulting in significant loss of color cues or the inability to maintain and leverage the potential relationships between color channels, thereby affecting the effectiveness of face recognition.

Recently, quaternions [15] and reduced biquaternions (RB) [16], [17], both four-dimensional algebras, have gained widespread attention as highly suitable tools for representing color pixels. They both contain one real part and three imaginary parts. When representing color pixels, the RGB channels are usually encoded in the three imaginary parts, thus treating the color pixel as an integrated entity. This allows the potential relationships between the color channels to be fully preserved and utilized. In particular, color image processing based on quaternions has recently been the subject of extensive research, such as quaternion matrix low-rank approximation for color image inpainting and color image denoising [18]–[21], quaternion sparse representation for color face recognition [11], quaternion dynamic mode decomposition for foreground-background separation in color videos [22], *etc.* Similarly, as a commutative four-dimensional algebra, RB, while not as maturely researched as quaternions, have recently achieved sig-

Jifei Miao is with the School of Mathematics and Statistics, Yunnan University, Kunming, Yunnan, 650091, China (e-mail: jifmiao@163.com).

Junjun Pan and Michael K. Ng are with the Department of Mathematics, Hong Kong Baptist University, Kowloon Tong, Hong Kong, China (e-mail: junjunpan@hkbu.edu.hk; michael-ng@hkbu.edu.hk).

nificant results in color image processing, such as those in studies [23]–[25].

Due to the superior structure of quaternions, some authors have recently started exploring the NMF problem on quaternions. Flamant et al. in [26] provided the first definition of quaternion non-negative matrix factorization (QNMF), but this model is designed for polarized signals and is not suitable for color image processing. To address color images, Ke et al. in [27] defined the quasi non-negative quaternion matrix (QNQM) and proposed a quasi non-negative quaternion matrix factorization (QN-QMF) model. However, due to the characteristics of quaternion multiplication, the QNQM model is theoretically difficult to ensure that the product of two quasi non-negative quaternion factor matrices is still a quasi non-negative quaternion matrix. To address this issue, we introduce the concept of the non-negative RB matrix and apply its multiplication properties to propose a non-negative RB matrix factorization (NRBMF) model. As far as we know, the NMF problem on RB has not been studied yet. A detailed introduction can be found in Subsection I-B and Subsection I-C below. Before that, we first present some notations used throughout this paper.

#### A. Notations

In this paper,  $\mathbb{R}$ ,  $\mathbb{C}$ ,  $\mathbb{Q}$ , and  $\mathbb{RB}$  respectively denote the real space, complex space, quaternion space, and RB space. Specifically, the set  $\mathbb{R}_+$  is defined as  $\mathbb{R}_+ = \{a \in \mathbb{R} | a = \max(0, a)\}$ . A scalar, a vector, and a matrix are written as  $a$ ,  $\mathbf{a}$ , and  $\mathbf{A}$  respectively.  $\hat{a}$ ,  $\hat{\mathbf{a}}$ , and  $\hat{\mathbf{A}}$  respectively represent a quaternion scalar, a quaternion vector, and a quaternion matrix.  $\tilde{a}$ ,  $\tilde{\mathbf{a}}$ , and  $\tilde{\mathbf{A}}$  respectively represent an RB scalar, an RB vector, and an RB matrix. To distinguish, we use bold  $\mathbf{i}, \mathbf{j}, \mathbf{k}$ , to represent the imaginary units of quaternions and  $i, j, k$  to represent the imaginary units of RB.  $\text{Im}_i(\cdot)$ ,  $\text{Im}_j(\cdot)$ , and  $\text{Im}_k(\cdot)$  are used to extract the three imaginary parts of the quaternion.  $\text{Im}_i(\cdot)$ ,  $\text{Im}_j(\cdot)$ , and  $\text{Im}_k(\cdot)$  are used to extract the three imaginary parts of the RB, and  $\text{Re}(\cdot)$  is used to extract the real part of the quaternion or the RB.  $(\cdot)^*$ ,  $(\cdot)^T$ ,  $(\cdot)^H$ , and  $(\cdot)^{-1}$  denote the conjugate, transpose, conjugate transpose, and inverse operations respectively.  $\otimes$  denotes the element-wise product between RB matrices. We simply use MATLAB command  $\text{vec}(\cdot)$  to vectorize a matrix, and  $\text{cond}(\cdot)$  to represent the condition number of a matrix.

#### B. Related Work and Motivation

The first work extending NMF to quaternions is called QNMF, proposed in [26]:

**Definition 1.** (QNMF [26]) For a set  $\mathbb{Q}_S \triangleq \{\hat{q} \in \mathbb{Q} | \text{Re}(\hat{q}) \geq 0, \text{Im}_i(\hat{q})^2 + \text{Im}_j(\hat{q})^2 + \text{Im}_k(\hat{q})^2 \leq \text{Re}(\hat{q})^2\}$ , QNMF of a given  $\mathbf{X} \in \mathbb{Q}_S^{M \times N}$  is defined as

$$\mathbf{X} = \mathbf{\hat{W}}\mathbf{H},$$

where  $\mathbf{\hat{W}} \in \mathbb{Q}_S^{M \times l}$ ,  $\mathbf{H} \in \mathbb{R}_+^{l \times N}$ , and  $l$  is a pre-specified positive integer such that  $l < \min(M, N)$ .

The QNMF model is specifically tailored for polarized signals, where quaternion matrices are used to represent the Stokes vector. However, for color images, the definition of QNMF is not suitable because the channel information of color images typically does not satisfy the set  $\mathbb{Q}_S$ .

To process color images, the authors in [27] defined the following QNQM set and a QNQM model:

**Definition 2.** (QNQM [27]) A quaternion matrix  $\hat{\mathbf{Q}} = \mathbf{Q}_0 + \mathbf{Q}_1\mathbf{i} + \mathbf{Q}_2\mathbf{j} + \mathbf{Q}_3\mathbf{k}$  is called the QNQM if  $\mathbf{Q}_1$ ,  $\mathbf{Q}_2$ , and  $\mathbf{Q}_3$  are real non-negative matrices, that is

$$\mathbf{Q}_1 \geq 0, \quad \mathbf{Q}_2 \geq 0, \quad \mathbf{Q}_3 \geq 0.$$

The set of QNQM is denoted by  $\mathbb{Q}_+^{M \times N}$ .

**Definition 3.** (QNQM [27]) For a given quaternion matrix  $\mathbf{X} = \mathbf{X}_0 + \mathbf{X}_1\mathbf{i} + \mathbf{X}_2\mathbf{j} + \mathbf{X}_3\mathbf{k} \in \mathbb{Q}_+^{M \times N}$ , it finds the matrices  $\mathbf{\hat{W}} = \mathbf{W}_0 + \mathbf{W}_1\mathbf{i} + \mathbf{W}_2\mathbf{j} + \mathbf{W}_3\mathbf{k} \in \mathbb{Q}_+^{M \times l}$  and  $\mathbf{\hat{H}} = \mathbf{H}_0 + \mathbf{H}_1\mathbf{i} + \mathbf{H}_2\mathbf{j} + \mathbf{H}_3\mathbf{k} \in \mathbb{Q}_+^{l \times N}$  such that

$$\mathbf{X} = \mathbf{\hat{W}}\mathbf{\hat{H}}, \quad (1)$$

that is

$$\begin{aligned} \mathbf{X} = & (\mathbf{W}_0\mathbf{H}_0 - \mathbf{W}_1\mathbf{H}_1 - \mathbf{W}_2\mathbf{H}_2 - \mathbf{W}_3\mathbf{H}_3) \\ & + (\mathbf{W}_0\mathbf{H}_1 + \mathbf{W}_1\mathbf{H}_0 + \mathbf{W}_2\mathbf{H}_3 - \mathbf{W}_3\mathbf{H}_2)\mathbf{i} \\ & + (\mathbf{W}_0\mathbf{H}_2 - \mathbf{W}_1\mathbf{H}_3 + \mathbf{W}_2\mathbf{H}_0 + \mathbf{W}_3\mathbf{H}_1)\mathbf{j} \\ & + (\mathbf{W}_0\mathbf{H}_3 + \mathbf{W}_1\mathbf{H}_2 - \mathbf{W}_2\mathbf{H}_1 + \mathbf{W}_3\mathbf{H}_0)\mathbf{k}. \end{aligned} \quad (2)$$

**Remark 1.** For the settings defined in Definition 2 and Definition 3, there are two fatal drawbacks:

- 1) From (2), one can find that when  $\mathbf{\hat{W}} \in \mathbb{Q}_+^{M \times l}$  and  $\mathbf{\hat{H}} \in \mathbb{Q}_+^{l \times N}$ , (i.e.,  $\mathbf{W}_1 \geq 0, \mathbf{W}_2 \geq 0, \mathbf{W}_3 \geq 0, \mathbf{H}_1 \geq 0, \mathbf{H}_2 \geq 0, \mathbf{H}_3 \geq 0$ ), it is hard to guarantee that  $\mathbf{\hat{W}}\mathbf{\hat{H}} \in \mathbb{Q}_+^{M \times N}$  (i.e., each imaginary part on the right side of equation (2) is non-negative). Thus, the obtained  $\mathbf{\hat{W}}$  and  $\mathbf{\hat{H}}$  are difficult to be the true solutions of (1).
- 2) The definition of QNQM does not restrict the non-negativity of the real part of the quaternion matrix, which will make the real part lack interpretability. In specific applications, such as color face recognition, the real part of the basis matrix  $\mathbf{\hat{W}}$  and encodings  $\mathbf{\hat{H}}$  containing negative entries cannot be reasonably explained or utilized.

Remark 1 above is the main motivation for proposing NMF on RB in this paper. We elaborate on the main contributions of this paper in Subsection I-C below.

### C. Contributions and Outline of This Paper

In this paper, in order to overcome the two potential drawbacks of QNQMF as outlined in Remark 1, we utilize the multiplication properties of RB algebra and propose an NRBMF model. The main contributions of this paper are summarized as follows:

- To process color images, we extend NMF to RB by introducing the concept of non-negative RB matrices and developing the NRBMF model. The proposed NRBMF model effectively overcomes the two drawbacks of QNQMF highlighted in Remark 1, thereby establishing a novel theoretical tool for color image processing.
- We propose a method for computing the gradient of a real-valued function with RB matrices as variables and develop an efficient RB projected gradient algorithm for the NRBMF optimization problem. Additionally, a convergence analysis of the algorithm has been provided.
- We apply the proposed NRBMF model to color face recognition. Unlike the QNQMF model in [27] that requires pure quaternion matrices with zero real parts, our NRBMF model accommodates RB matrices with non-zero real parts. Specifically, we encode the average RGB value of color face data into the real part of the RB matrix, eliminating the need to project onto pure RB matrices during optimization.

The rest paper is organized as follows. In Section II, we introduce RB algebra and RB matrices, and propose a method for computing the gradient of a real-valued function with RB matrices as variables. Section III presents the NRBMF model and provides the RB projected gradient algorithm for the NRBMF optimization problem, along with convergence analysis of the algorithm. Section IV gives the specific process of color face recognition based on NRBMF. Section V validates the effectiveness of the proposed method in color face recognition. The conclusion is ultimately provided in Section VI.

## II. PRELIMINARY

In this section, we will introduce RB algebra, RB matrices, and propose a method for computing the gradient of a real function with RB matrices as variables.

### A. Reduced Biquaternion

An RB number  $\ddot{q} \in \mathbb{RB}$  is defined as [17], [28], [29]:

$$\ddot{q} = q_0 + q_1 i + q_2 j + q_3 k, \quad (3)$$

where  $q_l \in \mathbb{R}$  ( $l = 0, 1, 2, 3$ ), and  $i, j, k$  are imaginary units satisfying

$$\begin{cases} i^2 = k^2 = -j^2 = -1, \\ ij = ji = k, jk = kj = i, ki = ik = -j. \end{cases} \quad (4)$$

The rules mentioned in (4) ensure the multiplication of two RB numbers to be commutative, which is different from the non-commutativity of quaternion multiplication. This is because the imaginary units of quaternions obey the following rules of operation [15]:

$$\begin{cases} i^2 = j^2 = k^2 = -1, \\ ij = -ji = k, jk = -kj = i, ki = -ik = j. \end{cases} \quad (5)$$

The conjugate and modulus of an RB number  $\ddot{q} \in \mathbb{RB}$  are defined as [30], [31]:

$$\ddot{q}^* = q_0 - q_1 i + q_2 j - q_3 k, \quad |\ddot{q}| = \sqrt{q_0^2 + q_1^2 + q_2^2 + q_3^2}.$$

There are two special RB numbers  $e_1$  and  $e_2$  [32], where

$$\begin{aligned} e_1 &= (1 + j)/2, \quad e_2 = (1 - j)/2, \quad \text{and } e_1 e_2 = 0, \\ e_1^n &= e_1^{n-1} = \dots = e_1^2 = e_1, \\ e_2^n &= e_2^{n-1} = \dots = e_2^2 = e_2. \end{aligned} \quad (6)$$

Therefore,  $e_1$  and  $e_2$  are both idempotent elements ( $e_1^2 = e_1$ ,  $e_2^2 = e_2$ ) and divisors of zero. Any RB number with the form  $c_1 e_1$  or  $c_2 e_2$  is also a divisor of zero and does not have a multiplicative inverse (where  $c_1$  and  $c_2$  are any complex numbers). Hence, the RB system is not a complete division system [30]. However, this has almost no influence on signal and image processing applications [17].

Furthermore, any RB number  $\ddot{q} \in \mathbb{RB}$  can be represented using  $e_1$ - $e_2$  form [30] as

$$\begin{aligned} \ddot{q} &= q_0 + q_1 i + q_2 j + q_3 k \\ &= (q_0 + q_1 i) + (q_2 + q_3 i)j \\ &= q_a + q_b j = q_{a+b} e_1 + q_{a-b} e_2, \end{aligned}$$

where  $q_{a+b} = q_a + q_b = (q_0 + q_2) + (q_1 + q_3)i$  and  $q_{a-b} = q_a - q_b = (q_0 - q_2) + (q_1 - q_3)i$ .

### B. Reduced Biquaternion Matrix

An RB matrix  $\ddot{\mathbf{Q}} = (\ddot{q}_{mn}) \in \mathbb{RB}^{M \times N}$  is given by

$$\ddot{\mathbf{Q}} = \mathbf{Q}_0 + \mathbf{Q}_1 i + \mathbf{Q}_2 j + \mathbf{Q}_3 k,$$

where  $\mathbf{Q}_l \in \mathbb{R}^{M \times N}$  ( $l = 0, 1, 2, 3$ ).  $\ddot{\mathbf{Q}}^T = (\ddot{q}_{nm}) \in \mathbb{RB}^{N \times M}$ ,  $\ddot{\mathbf{Q}}^* = (\ddot{q}_{mn}^*) \in \mathbb{RB}^{M \times N}$ , and  $\ddot{\mathbf{Q}}^H = (\ddot{q}_{nm}^*) \in \mathbb{RB}^{N \times M}$  respectively represent the transpose, conjugate,

and conjugate transpose of  $\ddot{\mathbf{Q}} = (\ddot{q}_{mn}) \in \mathbb{RB}^{M \times N}$ . If  $\mathbf{Q}_0 = 0$ , we refer to  $\ddot{\mathbf{Q}}$  as a pure RB matrix. The inner product and Frobenius norm of RB matrices are defined as follows:

$$\langle \ddot{\mathbf{Q}}, \ddot{\mathbf{P}} \rangle = \sum_{m=1}^M \sum_{n=1}^N \ddot{q}_{mn}^* \ddot{p}_{mn},$$

$$\|\ddot{\mathbf{Q}}\|_F = \sqrt{\text{Re}[\langle \ddot{\mathbf{Q}}, \ddot{\mathbf{Q}} \rangle]} = \sqrt{\sum_{m=1}^M \sum_{n=1}^N |\ddot{q}_{mn}|^2}.$$

Any RB matrix  $\ddot{\mathbf{Q}} \in \mathbb{RB}^{M \times N}$  can be represented using  $e_1$ - $e_2$  form as

$$\ddot{\mathbf{Q}} = \mathbf{M}_1 e_1 + \mathbf{M}_2 e_2,$$

where  $\mathbf{M}_1 \in \mathbb{C}^{M \times N} = (\mathbf{Q}_0 + \mathbf{Q}_2) + (\mathbf{Q}_1 + \mathbf{Q}_3)i$ ,  $\mathbf{M}_2 \in \mathbb{C}^{M \times N} = (\mathbf{Q}_0 - \mathbf{Q}_2) + (\mathbf{Q}_1 - \mathbf{Q}_3)i$ .

### C. The Gradient of a Real Function Involving RB Matrix Variables

Before we introduce our NRBMF model, we will first present the gradient of real functions with RB matrix variables. This method is inspired by the quaternion version discussed in [33], [34].

**Definition 4.** Let  $f: \mathbb{RB}^{M \times N} \rightarrow \mathbb{R}$ ,  $\ddot{\mathbf{X}} = \mathbf{X}_0 + \mathbf{X}_1 i + \mathbf{X}_2 j + \mathbf{X}_3 k$ , where  $\mathbf{X}_l \in \mathbb{R}^{M \times N}$  ( $l = 0, 1, 2, 3$ ). If  $\frac{\partial f}{\partial \mathbf{X}_l}$  ( $l = 0, 1, 2, 3$ ) exists, we say  $f$  is differentiable, and we denote the gradient of  $f$  with respect to  $\ddot{\mathbf{X}}$  as

$$\nabla_{\ddot{\mathbf{X}}} f(\ddot{\mathbf{X}}) = \frac{\partial f}{\partial \mathbf{X}_0} + \frac{\partial f}{\partial \mathbf{X}_1} i + \frac{\partial f}{\partial \mathbf{X}_2} j + \frac{\partial f}{\partial \mathbf{X}_3} k. \quad (7)$$

Based on the Definition 4, we have the following theorem.

**Theorem 1.** Suppose that  $f: (\mathbb{RB}^{M \times l}, \mathbb{RB}^{l \times N}) \rightarrow \mathbb{R}$  be defined by  $f(\ddot{\mathbf{W}}, \ddot{\mathbf{H}}) = \frac{1}{2} \|\ddot{\mathbf{X}} - \ddot{\mathbf{W}}\ddot{\mathbf{H}}\|_F^2$ , where  $\ddot{\mathbf{W}} = \mathbf{W}_0 + \mathbf{W}_1 i + \mathbf{W}_2 j + \mathbf{W}_3 k \in \mathbb{RB}^{M \times l}$ ,  $\ddot{\mathbf{H}} = \mathbf{H}_0 + \mathbf{H}_1 i + \mathbf{H}_2 j + \mathbf{H}_3 k \in \mathbb{RB}^{l \times N}$ , and  $\ddot{\mathbf{X}} = \mathbf{X}_0 + \mathbf{X}_1 i + \mathbf{X}_2 j + \mathbf{X}_3 k \in \mathbb{RB}^{M \times N}$ , then

$$\begin{cases} \nabla_{\ddot{\mathbf{W}}} f(\ddot{\mathbf{W}}, \ddot{\mathbf{H}}) = (\ddot{\mathbf{W}}\ddot{\mathbf{H}} - \ddot{\mathbf{X}})\ddot{\mathbf{H}}^H, \\ \nabla_{\ddot{\mathbf{H}}} f(\ddot{\mathbf{W}}, \ddot{\mathbf{H}}) = \ddot{\mathbf{W}}^H(\ddot{\mathbf{W}}\ddot{\mathbf{H}} - \ddot{\mathbf{X}}). \end{cases} \quad (8)$$

The proof of Theorem 1 can be found in Section 1 of the Supplementary Materials.

### III. NON-NEGATIVE REDUCED BIQUATERNION MATRIX FACTORIZATION

In this section, we introduce the NRBMF model and discuss its corresponding optimization problem.

**Definition 5.** (Non-Negative RB Matrix) An RB matrix  $\ddot{\mathbf{Q}} = \mathbf{Q}_0 + \mathbf{Q}_1 i + \mathbf{Q}_2 j + \mathbf{Q}_3 k$  is called the non-negative

RB matrix if  $\mathbf{Q}_l$  ( $l = 0, 1, 2, 3$ ) are real non-negative matrices, that is

$$\mathbf{Q}_0 \geq 0, \quad \mathbf{Q}_1 \geq 0, \quad \mathbf{Q}_2 \geq 0, \quad \mathbf{Q}_3 \geq 0.$$

The set of non-negative RB matrices is denoted by  $\mathbb{RB}_+^{M \times N}$ . Specially, let the set composed of non-negative RB matrices with the first and third imaginary parts being zero be denoted as  $\mathbb{RB}_{+j}^{M \times N}$ , i.e., if  $\ddot{\mathbf{Q}} \in \mathbb{RB}_{+j}^{M \times N}$ , then  $\ddot{\mathbf{Q}}$  can be written as

$$\ddot{\mathbf{Q}} = \mathbf{Q}_0 + \mathbf{Q}_2 j,$$

where  $\mathbf{Q}_0 \geq 0$  and  $\mathbf{Q}_2 \geq 0$ .

**Definition 6.** (NRBMF) For a given RB matrix  $\ddot{\mathbf{X}} = \mathbf{X}_0 + \mathbf{X}_1 i + \mathbf{X}_2 j + \mathbf{X}_3 k \in \mathbb{RB}^{M \times N}$ , NRBMF is to find two RB matrices  $\ddot{\mathbf{W}} = \mathbf{W}_0 + \mathbf{W}_1 i + \mathbf{W}_2 j + \mathbf{W}_3 k \in \mathbb{RB}_+^{M \times l}$  and  $\ddot{\mathbf{H}} = \mathbf{H}_0 + \mathbf{H}_2 j \in \mathbb{RB}_{+j}^{l \times N}$  such that

$$\ddot{\mathbf{X}} = \ddot{\mathbf{W}}\ddot{\mathbf{H}}, \quad (9)$$

that is

$$\begin{aligned} \mathbf{X}_0 + \mathbf{X}_1 i + \mathbf{X}_2 j + \mathbf{X}_3 k = & (\mathbf{W}_0 \mathbf{H}_0 + \mathbf{W}_2 \mathbf{H}_2) \\ & + (\mathbf{W}_1 \mathbf{H}_0 + \mathbf{W}_3 \mathbf{H}_2) i \\ & + (\mathbf{W}_0 \mathbf{H}_2 + \mathbf{W}_2 \mathbf{H}_0) j \\ & + (\mathbf{W}_1 \mathbf{H}_2 + \mathbf{W}_3 \mathbf{H}_0) k, \end{aligned} \quad (10)$$

where  $l$  is a pre-specified positive integer such that  $l < \min(M, N)$ .

**Remark 2.** The proposed NRBMF model in (9) has the following main advantages:

- 1) From (10), one can find that when  $\ddot{\mathbf{W}} \in \mathbb{RB}_+^{M \times l}$  and  $\ddot{\mathbf{H}} \in \mathbb{RB}_{+j}^{l \times N}$  are non-negative RB matrix, NRBMF can always guarantee that  $\ddot{\mathbf{X}} \in \mathbb{RB}_+^{M \times N}$  is a non-negative RB matrix, which is different from (2) of QNQM.
- 2) As mentioned in Remark 1, the QNQM does not impose any constraints on the real parts of  $\ddot{\mathbf{X}}$ ,  $\ddot{\mathbf{W}}$ , and  $\ddot{\mathbf{H}}$ , which renders the real parts of them uninterpretable and not reasonably utilizable. In contrast, the NRBMF constrains the non-negativity of the real parts of  $\ddot{\mathbf{X}}$ ,  $\ddot{\mathbf{W}}$ , and  $\ddot{\mathbf{H}}$ , which addresses the drawbacks of the QNQM model.

Therefore, the conclusion is that the NRBMF model can fully address the two drawbacks of the QNQM model listed in Remark 1. Especially, one can see the interpretability of our NRBMF model from the color face recognition application in Section IV.

#### A. RB Optimization Problem

To solve the NRBMF in (9), we consider the following simple optimization problem:

$$\begin{aligned} \min f(\ddot{\mathbf{W}}, \ddot{\mathbf{H}}) &= \frac{1}{2} \|\ddot{\mathbf{X}} - \ddot{\mathbf{W}}\ddot{\mathbf{H}}\|_F^2 \\ \text{s.t. } \ddot{\mathbf{W}} &\in \mathbb{RB}_+^{M \times l}, \quad \ddot{\mathbf{H}} \in \mathbb{RB}_{+j}^{l \times N}. \end{aligned} \quad (11)$$

One can find that the above object function  $f(\ddot{\mathbf{W}}, \ddot{\mathbf{H}})$  is a real-valued function with two RB variables. Thus, the gradient of  $f(\ddot{\mathbf{W}}, \ddot{\mathbf{H}})$  with respect to  $\ddot{\mathbf{W}}$  and  $\ddot{\mathbf{H}}$  is given by (8).

### B. RB Projected Gradient Algorithm

In order to tackle the optimization problem in (11), we consider the following RB-ANNLS problem, which involves fixing one RB matrix and optimizing the other in an alternating fashion:

$$\begin{cases} \ddot{\mathbf{W}}_{t+1} = \arg \min_{\ddot{\mathbf{W}} \in \mathbb{RB}_+^{M \times l}} \frac{1}{2} \|\ddot{\mathbf{X}} - \ddot{\mathbf{W}} \ddot{\mathbf{H}}_t\|_F^2, \\ \ddot{\mathbf{H}}_{t+1} = \arg \min_{\ddot{\mathbf{H}} \in \mathbb{RB}_+^{l \times N}} \frac{1}{2} \|\ddot{\mathbf{X}} - \ddot{\mathbf{W}}_{t+1} \ddot{\mathbf{H}}\|_F^2. \end{cases} \quad (12)$$

Let  $\mathcal{P}_{\mathbb{RB}_+^{M \times N}}$  and  $\mathcal{P}_{\mathbb{RB}_+^{l \times N}}$  be two projections on  $\mathbb{RB}_+^{M \times N}$  and  $\mathbb{RB}_+^{l \times N}$ , which are defined as

$$\begin{aligned} \mathcal{P}_{\mathbb{RB}_+^{M \times N}}(\ddot{\mathbf{Q}}) &= \mathcal{P}_{\mathbb{R}_+^{M \times N}}(\mathbf{Q}_0) + \mathcal{P}_{\mathbb{R}_+^{M \times N}}(\mathbf{Q}_1)i \\ &\quad + \mathcal{P}_{\mathbb{R}_+^{M \times N}}(\mathbf{Q}_2)j + \mathcal{P}_{\mathbb{R}_+^{M \times N}}(\mathbf{Q}_3)k, \\ \mathcal{P}_{\mathbb{RB}_+^{l \times N}}(\ddot{\mathbf{Q}}) &= \mathcal{P}_{\mathbb{R}_+^{l \times N}}(\mathbf{Q}_0) + \mathcal{P}_{\mathbb{R}_+^{l \times N}}(\mathbf{Q}_2)j, \end{aligned}$$

where  $\mathcal{P}_{\mathbb{R}_+^{M \times N}}(\mathbf{Q}_l) = \max(\mathbf{Q}_l, 0)$ .

Obviously, for problem (12), the following standard RB projected gradient method can be applied:

$$\begin{cases} \ddot{\mathbf{W}}_{t+1} = \mathcal{P}_{\mathbb{RB}_+^{M \times l}}(\ddot{\mathbf{W}}_t - \alpha \nabla_{\ddot{\mathbf{W}}} f(\ddot{\mathbf{W}}_t, \ddot{\mathbf{H}}_t)), \\ \ddot{\mathbf{H}}_{t+1} = \mathcal{P}_{\mathbb{RB}_+^{l \times N}}(\ddot{\mathbf{H}}_t - \beta \nabla_{\ddot{\mathbf{H}}} f(\ddot{\mathbf{W}}_{t+1}, \ddot{\mathbf{H}}_t)), \end{cases} \quad (13)$$

where  $\alpha$  and  $\beta$  are the step sizes. To ensure the effective convergence of the algorithm, the selection of step size is necessary. In this paper, we use the Armijo linear search method [35], [36] to determine the step size of each update, and give the algorithm procedure as shown in Table I.

Actually, finding the appropriate values for  $\alpha_t$  and  $\beta_t$  is the most time-consuming task in Table I, so one should check as few step sizes as possible. To achieve this, we employ a technique that uses  $\alpha_{t-1}$  and  $\beta_{t-1}$  as the initial guess and then adjusts them to find the maximum  $\mu^{dt}$  and  $\mu^{st}$  that satisfy conditions (14) and (15), respectively. This approach leverages the similarity between  $\alpha_{t-1}$  and  $\alpha_t$  ( $\beta_{t-1}$  and  $\beta_t$ ) [36], [37]. At times, a larger step size can more effectively project variables to their bounds within a single iteration. For this, we use a better initial guess for  $\alpha$  and  $\beta$  in each iteration, resulting in the RB improved projected gradient (RBIPG) algorithm presented in Table II, which is the algorithm ultimately adopted in this study.

TABLE I: RB projected gradient method for RB-ANNLS problem (12).

---

**Input:** Given an RB matrix  $\ddot{\mathbf{X}} \in \mathbb{RB}_+^{M \times N}$ ,  $l < \min(M, N)$ ,  $tol = 1e^{-4}$ ,  $\mu = 0.1$ ,  $\sigma = 0.001$ , and maximum number of iterations  $I$ .

- 1: **Initialize**  $\ddot{\mathbf{W}}_0 \in \mathbb{RB}_+^{M \times l}$  and  $\ddot{\mathbf{H}}_0 \in \mathbb{RB}_+^{l \times N}$ , are randomly initialized;  $t = 0$ .
- 2: **Repeat**
- 3: % Update  $\ddot{\mathbf{W}}$
- 4: Compute  $\nabla_{\ddot{\mathbf{W}}} f(\ddot{\mathbf{W}}_t, \ddot{\mathbf{H}}_t) = (\ddot{\mathbf{W}}_t \ddot{\mathbf{H}}_t - \ddot{\mathbf{X}}) \ddot{\mathbf{H}}_t^H$ ;
- 5: Update  $\ddot{\mathbf{W}}_{t+1} = \mathcal{P}_{\mathbb{RB}_+^{M \times l}}(\ddot{\mathbf{W}}_t - \alpha_t \nabla_{\ddot{\mathbf{W}}} f(\ddot{\mathbf{W}}_t, \ddot{\mathbf{H}}_t))$ , where  $\alpha_t = \mu^{dt}$ , and  $d_t$  is the first non-negative integer  $d$  for which
 
$$\begin{aligned} & f(\ddot{\mathbf{W}}_{t+1}, \ddot{\mathbf{H}}_t) - f(\ddot{\mathbf{W}}_t, \ddot{\mathbf{H}}_t) \\ & \leq \sigma \text{Re} \left( \langle \nabla_{\ddot{\mathbf{W}}} f(\ddot{\mathbf{W}}_t, \ddot{\mathbf{H}}_t), \ddot{\mathbf{W}}_{t+1} - \ddot{\mathbf{W}}_t \rangle \right). \end{aligned} \quad (14)$$
- 6: % Update  $\ddot{\mathbf{H}}$
- 7: Compute  $\nabla_{\ddot{\mathbf{H}}} f(\ddot{\mathbf{W}}_{t+1}, \ddot{\mathbf{H}}_t) = \ddot{\mathbf{W}}_{t+1}^H (\ddot{\mathbf{W}}_{t+1} \ddot{\mathbf{H}}_t - \ddot{\mathbf{X}})$ ;
- 8: Update  $\ddot{\mathbf{H}}_{t+1} = \mathcal{P}_{\mathbb{RB}_+^{l \times N}}(\ddot{\mathbf{H}}_t - \beta_t \nabla_{\ddot{\mathbf{H}}} f(\ddot{\mathbf{W}}_{t+1}, \ddot{\mathbf{H}}_t))$ , where  $\beta_t = \mu^{st}$ , and  $s_t$  is the first non-negative integer  $s$  for which
 
$$\begin{aligned} & f(\ddot{\mathbf{W}}_{t+1}, \ddot{\mathbf{H}}_{t+1}) - f(\ddot{\mathbf{W}}_{t+1}, \ddot{\mathbf{H}}_t) \\ & \leq \sigma \text{Re} \left( \langle \nabla_{\ddot{\mathbf{H}}} f(\ddot{\mathbf{W}}_{t+1}, \ddot{\mathbf{H}}_t), \ddot{\mathbf{H}}_{t+1} - \ddot{\mathbf{H}}_t \rangle \right). \end{aligned} \quad (15)$$
- 9:  $t \leftarrow t + 1$ .
- 10: **Until**  $\frac{\|\ddot{\mathbf{W}}_t \ddot{\mathbf{H}}_t - \ddot{\mathbf{W}}_{t-1} \ddot{\mathbf{H}}_{t-1}\|_F}{\|\ddot{\mathbf{W}}_{t-1} \ddot{\mathbf{H}}_{t-1}\|_F} < tol$  or  $t - 1 > I$ .

**Output:**  $\ddot{\mathbf{W}}_t \in \mathbb{RB}_+^{M \times l}$  and  $\ddot{\mathbf{H}}_t \in \mathbb{RB}_+^{l \times N}$ .

---

TABLE II: RBIPG for RB-ANNLS problem (12).

---

**Input:** Given an RB matrix  $\ddot{\mathbf{X}} \in \mathbb{RB}_+^{M \times N}$ ,  $l < \min(M, N)$ ,  $tol = 1e^{-4}$ ,  $\delta = 10$ , and maximum number of iterations  $I$ .

- 1: **Initialize**  $\ddot{\mathbf{W}}_0 \in \mathbb{RB}_+^{M \times l}$  and  $\ddot{\mathbf{H}}_0 \in \mathbb{RB}_+^{l \times N}$ , are randomly initialized;  $t = 0$ ; Step size  $\alpha_0 = \beta_0 = 1$ .
- 2: **Repeat**
- 3: % Update  $\ddot{\mathbf{W}}$
- 4: Compute  $\nabla_{\ddot{\mathbf{W}}} f(\ddot{\mathbf{W}}_t, \ddot{\mathbf{H}}_t) = (\ddot{\mathbf{W}}_t \ddot{\mathbf{H}}_t - \ddot{\mathbf{X}}) \ddot{\mathbf{H}}_t^H$ ;
- 5: Assign  $\alpha_t \leftarrow \alpha_{t-1}$ .
- 6: If  $\alpha_t$  satisfies (14), repeatedly increase it by  $\alpha_t = \alpha_t * \delta$  until  $\alpha_t$  does not satisfy (14). Else, repeatedly decrease  $\alpha_t$  by  $\alpha_t = \alpha_t / \delta$  until  $\alpha_t$  satisfies (14).
- 7: Update  $\ddot{\mathbf{W}}_{t+1} = \mathcal{P}_{\mathbb{RB}_+^{M \times l}}(\ddot{\mathbf{W}}_t - \alpha_t \nabla_{\ddot{\mathbf{W}}} f(\ddot{\mathbf{W}}_t, \ddot{\mathbf{H}}_t))$ .
- 8: % Update  $\ddot{\mathbf{H}}$
- 9: Compute  $\nabla_{\ddot{\mathbf{H}}} f(\ddot{\mathbf{W}}_{t+1}, \ddot{\mathbf{H}}_t) = \ddot{\mathbf{W}}_{t+1}^H (\ddot{\mathbf{W}}_{t+1} \ddot{\mathbf{H}}_t - \ddot{\mathbf{X}})$ ;
- 10: Assign  $\beta_t \leftarrow \beta_{t-1}$ .
- 11: If  $\beta_t$  satisfies (15), repeatedly increase it by  $\beta_t = \beta_t * \delta$  until  $\beta_t$  does not satisfy (15). Else, repeatedly decrease  $\beta_t$  by  $\beta_t = \beta_t / \delta$  until  $\beta_t$  satisfies (15).
- 12: Update  $\ddot{\mathbf{H}}_{t+1} = \mathcal{P}_{\mathbb{RB}_+^{l \times N}}(\ddot{\mathbf{H}}_t - \beta_t \nabla_{\ddot{\mathbf{H}}} f(\ddot{\mathbf{W}}_{t+1}, \ddot{\mathbf{H}}_t))$ .
- 13:  $t \leftarrow t + 1$ .
- 14: **Until**  $\frac{\|\ddot{\mathbf{W}}_t \ddot{\mathbf{H}}_t - \ddot{\mathbf{W}}_{t-1} \ddot{\mathbf{H}}_{t-1}\|_F}{\|\ddot{\mathbf{W}}_{t-1} \ddot{\mathbf{H}}_{t-1}\|_F} < tol$  or  $t - 1 > I$ .

**Output:**  $\ddot{\mathbf{W}}_t \in \mathbb{RB}_+^{M \times l}$  and  $\ddot{\mathbf{H}}_t \in \mathbb{RB}_+^{l \times N}$ .

---

### C. Convergence analysis

We first present the Karush-Kuhn-Tucker (KKT) conditions for the NRBMF optimization problem (11) in the following property.

**Property 1.**  $(\ddot{\mathbf{W}}^*, \ddot{\mathbf{H}}^*)$  is a stationary point of (11) if and only if

$$\begin{cases} \ddot{\mathbf{W}}^* \in \mathbb{RB}_+^{M \times l}, \ddot{\mathbf{H}}^* \in \mathbb{RB}_+^{l \times N}; \\ \nabla_{\ddot{\mathbf{W}}} f(\ddot{\mathbf{W}}^*, \ddot{\mathbf{H}}^*) \in \mathbb{RB}_+^{M \times l}, \nabla_{\ddot{\mathbf{H}}} f(\ddot{\mathbf{W}}^*, \ddot{\mathbf{H}}^*) \in \mathbb{RB}_+^{l \times N}; \\ \text{Re}(\ddot{\mathbf{W}}^*) \otimes \text{Re}(\nabla_{\ddot{\mathbf{W}}} f(\ddot{\mathbf{W}}^*, \ddot{\mathbf{H}}^*)) = 0, \\ \text{Im}_\eta(\ddot{\mathbf{W}}^*) \otimes \text{Im}_\eta(\nabla_{\ddot{\mathbf{W}}} f(\ddot{\mathbf{W}}^*, \ddot{\mathbf{H}}^*)) = 0, \eta = i, j, k; \\ \text{Re}(\ddot{\mathbf{H}}^*) \otimes \text{Re}(\nabla_{\ddot{\mathbf{H}}} f(\ddot{\mathbf{W}}^*, \ddot{\mathbf{H}}^*)) = 0, \\ \text{Im}_j(\ddot{\mathbf{H}}^*) \otimes \text{Im}_j(\nabla_{\ddot{\mathbf{H}}} f(\ddot{\mathbf{W}}^*, \ddot{\mathbf{H}}^*)) = 0. \end{cases} \quad (16)$$

The proof of Property 1 can be found in Section 2 of the Supplementary Materials.

**Corollary 1.**  $(\ddot{\mathbf{W}}^*, \ddot{\mathbf{H}}^*)$  is a stationary point of (11) if and only if

$$\begin{cases} \text{Re}(\langle \nabla_{\ddot{\mathbf{W}}} f(\ddot{\mathbf{W}}^*, \ddot{\mathbf{H}}^*), \ddot{\mathbf{M}} - \ddot{\mathbf{W}}^* \rangle) \geq 0, \quad \forall \ddot{\mathbf{M}} \in \mathbb{RB}_+^{M \times l}, \\ \text{Re}(\langle \nabla_{\ddot{\mathbf{H}}} f(\ddot{\mathbf{W}}^*, \ddot{\mathbf{H}}^*), \ddot{\mathbf{N}} - \ddot{\mathbf{H}}^* \rangle) \geq 0, \quad \forall \ddot{\mathbf{N}} \in \mathbb{RB}_+^{l \times N}. \end{cases} \quad (17)$$

The proof of Corollary 1 can be found in Section 3 of the Supplementary Materials.

For the sake of analytical convenience, we primarily examine the convergence of RBPG as presented in Table I. RBIPG in Table II represents a specific case of RBPG with particular step sizes, and its convergence properties naturally coincide with those of RBPG.

**Theorem 2.** The sequence of objective function values  $\{f(\ddot{\mathbf{W}}_t, \ddot{\mathbf{H}}_t)\}_{t=1}^\infty$  generated by RBPG in Table I is nonincreasing.

The proof of Theorem 2 can be found in Section 4 of the Supplementary Materials.

**Theorem 3.** Suppose  $\{f(\ddot{\mathbf{W}}_t, \ddot{\mathbf{H}}_t)\}_{t=1}^\infty$  is the sequence generated by RBPG in Table I. If

$$\lim_{t \rightarrow +\infty} \ddot{\mathbf{W}}_t = \ddot{\mathbf{W}}^* \quad \text{and} \quad \lim_{t \rightarrow +\infty} \ddot{\mathbf{H}}_t = \ddot{\mathbf{H}}^*,$$

then  $(\ddot{\mathbf{W}}^*, \ddot{\mathbf{H}}^*)$  is a stationary point of (11).

The proof of Theorem 3 can be found in Section 5 of the Supplementary Materials.

## IV. APPLICATIONS IN COLOR FACE RECOGNITION

To leverage color information in face images and the advantages of the NRBMF model, this section proposes a method for color face recognition based on NRBMF theory.

For a color face image, assuming  $\mathbf{X}_R \in \mathbb{R}^{M \times N}$ ,  $\mathbf{X}_G \in \mathbb{R}^{M \times N}$ , and  $\mathbf{X}_B \in \mathbb{R}^{M \times N}$  represent the values of its red, green, and blue channels, respectively. we consider representing it by the following full RB matrix:

$$\ddot{\mathbf{X}} = \mathbf{X}_{av} + \mathbf{X}_R i + \mathbf{X}_G j + \mathbf{X}_B k, \quad (18)$$

where  $\mathbf{X}_{av} = (\mathbf{X}_R + \mathbf{X}_G + \mathbf{X}_B)/3$  denotes the average values of the three color channels. Figure 1 visually demonstrates this representation strategy more clearly.

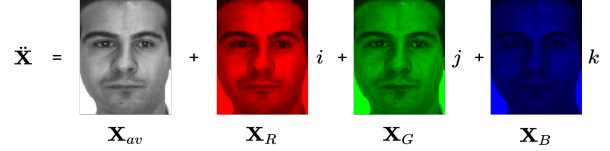


Fig. 1: Color Face Image Represented by RB Matrix.

**Remark 3.** According to the NRBMF model, we have

$$\begin{aligned} & \mathbf{X}_{av} + \mathbf{X}_R i + \mathbf{X}_G j + \mathbf{X}_B k \\ &= (\mathbf{W}_0 + \mathbf{W}_1 i + \mathbf{W}_2 j + \mathbf{W}_3 k)(\mathbf{H}_0 + \mathbf{H}_2 j) \\ &= (\mathbf{W}_0 \mathbf{H}_0 + \mathbf{W}_2 \mathbf{H}_2) + (\mathbf{W}_1 \mathbf{H}_0 + \mathbf{W}_3 \mathbf{H}_2) i \\ & \quad + (\mathbf{W}_0 \mathbf{H}_2 + \mathbf{W}_2 \mathbf{H}_0) j + (\mathbf{W}_1 \mathbf{H}_2 + \mathbf{W}_3 \mathbf{H}_0) k, \end{aligned} \quad (19)$$

where  $\mathbf{W}_0$ ,  $\mathbf{W}_1$ ,  $\mathbf{W}_2$ , and  $\mathbf{W}_3$  can be naturally interpreted as the four-channel information of the basis face images,  $\mathbf{H}_0$  and  $\mathbf{H}_1$  can be regarded as a set of combined encoding coefficient matrices. One can find that each channel of  $\ddot{\mathbf{X}}$  is composed of two channels of the basis matrix  $\ddot{\mathbf{W}}$ , which is beneficial for the complementarity of information between channels. Moreover, the encoding coefficient matrices of each channel of  $\ddot{\mathbf{X}}$  share the common combination of  $\mathbf{H}_0$  and  $\mathbf{H}_1$ , which helps to simulate the potential relationships between color channels.

**Remark 4.** Our setting in (18) differs from that in [27], where they only consider  $\mathbf{X}_R$ ,  $\mathbf{X}_G$ , and  $\mathbf{X}_B$ , representing color face images as pure quaternion matrices. We represent it as a full RB matrix for two main reasons.

- 1) The inclusion of  $\mathbf{X}_{av}$  does not introduce any additional information. Encoding it in the real part of the RB matrix makes rational use of the real part, thus can eliminate the constraint that the real part of  $\ddot{\mathbf{W}}\ddot{\mathbf{H}}$  must be zero during optimization.
- 2) From (19), it can be observed that if we use a pure RB matrix to encode the color face image (i.e., the real part of  $\ddot{\mathbf{X}}$  is zero), then as the objective function is minimized,  $(\mathbf{W}_0 \mathbf{H}_0 + \mathbf{W}_2 \mathbf{H}_2)$  in (19) will tend towards zero. This will cause the information in the two channels of the basis

matrix,  $\mathbf{W}_0$  and  $\mathbf{W}_2$ , to diminish, thereby may affect the face recognition capability.

Below, we give the detailed process of performing color face recognition using the proposed NRBMF model:

1) **Preparing the training and testing data.** All color faces are represented as an RB matrix in the form of (18). Assuming we have  $K$  training samples  $\ddot{\mathbf{T}}_k \in \mathbb{RB}_+^{M \times N}$ ,  $k = 1, 2, \dots, K$ , and  $S$  testing samples  $\ddot{\mathbf{P}}_s \in \mathbb{RB}_+^{M \times N}$ ,  $s = 1, 2, \dots, S$ , let  $\ddot{\mathbf{X}} = [\ddot{\mathbf{t}}_1, \ddot{\mathbf{t}}_2, \dots, \ddot{\mathbf{t}}_K] \in \mathbb{RB}_+^{M \times N \times K}$ ,  $\ddot{\mathbf{G}} = [\ddot{\mathbf{p}}_1, \ddot{\mathbf{p}}_2, \dots, \ddot{\mathbf{p}}_S] \in \mathbb{RB}_+^{M \times N \times S}$ , where  $\ddot{\mathbf{t}}_k = \text{vec}(\ddot{\mathbf{T}}_k) \in \mathbb{RB}_+^{MN \times 1}$  for  $k = 1, 2, \dots, K$  and  $\ddot{\mathbf{p}}_s = \text{vec}(\ddot{\mathbf{P}}_s) \in \mathbb{RB}_+^{MN \times 1}$  for  $s = 1, 2, \dots, S$ .

2) **Obtaining the basis matrix and encoding coefficients.** For the given  $\ddot{\mathbf{X}} \in \mathbb{RB}_+^{M \times N \times K}$  and  $l$ , we apply RBIPG to obtain the basis matrix  $\ddot{\mathbf{W}} \in \mathbb{RB}_+^{M \times N \times l}$  and encoding coefficients  $\ddot{\mathbf{H}} \in \mathbb{RB}_+^{l \times K}$ . Once  $\ddot{\mathbf{W}}$  and  $\ddot{\mathbf{H}}$  are found, and, since  $\ddot{\mathbf{X}} = \ddot{\mathbf{W}}\ddot{\mathbf{H}}$ , the encodings,  $\ddot{\mathbf{h}}_k^{(train)}$  of each training face  $\ddot{\mathbf{t}}_k$ , from [31], is given by  $\ddot{\mathbf{h}}_k^{(train)} = (\ddot{\mathbf{W}}^H \ddot{\mathbf{W}})^{-1} \ddot{\mathbf{W}}^H \ddot{\mathbf{t}}_k$ .

3) **Color face recognition.** For a given test color face  $\ddot{\mathbf{p}}_s \in \mathbb{RB}_+^{M \times N \times 1}$ , based on the basis matrix  $\ddot{\mathbf{W}} \in \mathbb{RB}_+^{M \times N \times l}$ , the corresponding encodings  $\ddot{\mathbf{h}}_s^{test} \in \mathbb{RB}^{l \times 1}$  can be obtained by  $\ddot{\mathbf{h}}_s^{test} = (\ddot{\mathbf{W}}^H \ddot{\mathbf{W}})^{-1} \ddot{\mathbf{W}}^H \ddot{\mathbf{p}}_s$ .

The following cosine similarity measure is utilized to gauge the similarity between the test encodings and the training encodings:

$$d_k = \frac{\text{Re}(\langle \ddot{\mathbf{h}}_k^{(train)}, \ddot{\mathbf{h}}_s^{test} \rangle)}{\|\ddot{\mathbf{h}}_k^{(train)}\|_F \|\ddot{\mathbf{h}}_s^{test}\|_F}, \quad k = 1, 2, \dots, K. \quad (20)$$

Suppose  $d_{k^*} = \max\{d_1, d_2, \dots, d_K\}$ , then the test color face  $\ddot{\mathbf{p}}_s$  is considered to belong to the subject that the training sample  $\ddot{\mathbf{t}}_{k^*}$  belongs to.

**Remark 5.** In steps 2) and 3), we assume  $\ddot{\mathbf{W}}^H \ddot{\mathbf{W}} = \mathbf{M}_1 e_1 + \mathbf{M}_2 e_2$ . The inverse of  $\ddot{\mathbf{W}}^H \ddot{\mathbf{W}}$  exists, if and only if the inverses of  $\mathbf{M}_1$  and  $\mathbf{M}_2$  exist. And, the inverse of  $\ddot{\mathbf{W}}^H \ddot{\mathbf{W}}$  is  $(\ddot{\mathbf{W}}^H \ddot{\mathbf{W}})^{-1} = \mathbf{M}_1^{-1} e_1 + \mathbf{M}_2^{-1} e_2$  [30]. If  $\max\{\text{cond}(\mathbf{M}_1), \text{cond}(\mathbf{M}_2)\} > 1e^{15}$ , the RB gradient descent method is used, in steps 2) and 3), to solve the RB least-square problems  $\min_{\ddot{\mathbf{h}} \in \mathbb{RB}^{l \times 1}} \|\ddot{\mathbf{t}}_k - \ddot{\mathbf{W}}\ddot{\mathbf{h}}\|_F^2$  and  $\min_{\ddot{\mathbf{h}} \in \mathbb{RB}^{l \times 1}} \|\ddot{\mathbf{p}}_s - \ddot{\mathbf{W}}\ddot{\mathbf{h}}\|_F^2$  to obtain  $\ddot{\mathbf{h}}_k^{(train)}$  and  $\ddot{\mathbf{h}}_s^{test}$ .

## V. NUMERICAL EXPERIMENTS OF COLOR FACE RECOGNITION

In this section, extensive experiments are conducted to demonstrate the effectiveness and superiority of the proposed NRBMF model for color face recognition. All the experiments are run in MATLAB 2014b under

Windows 10 on a personal computer with a 1.60GHz CPU and 8GB memory.

We compare with the following several methods:

- **RBIPG-full:** The RBIPG algorithm in Table II for NRBMF. The term ‘full’ means representing the color face as shown in (18), where the real part of  $\ddot{\mathbf{X}}$  is  $\mathbf{X}_{av}$ .
- **RBIPG-pure:** The term ‘pure’ means that the real part of  $\ddot{\mathbf{X}}$  is a zero matrix.
- **QIPG-full** [27]: The quaternion improved projected gradient (QIPG) algorithm for QNQMf. Note that the QNQMf model does not consider the real part of the quaternion matrix. However, for a fair comparison, in this scenario, we encode  $\mathbf{X}_{av}$  as the real part of the quaternion matrix  $\ddot{\mathbf{X}}$ .
- **QIPG-pure** [27]: The same as its original setting, i.e., the real part of quaternion matrix  $\ddot{\mathbf{X}}$  is zero.
- **RIPG-full** [36]: The real improved projected gradient (RIPG) algorithm for NMF. In this setting, we perform NMF on  $\mathbf{X}_{av}$ ,  $\mathbf{X}_R$ ,  $\mathbf{X}_G$ , and  $\mathbf{X}_B$  respectively, i.e.,  $\mathbf{X}_{av} = \mathbf{W}_{av}\mathbf{H}_{av}$ ,  $\mathbf{X}_R = \mathbf{W}_R\mathbf{H}_R$ ,  $\mathbf{X}_G = \mathbf{W}_G\mathbf{H}_G$ ,  $\mathbf{X}_B = \mathbf{W}_B\mathbf{H}_B$ . The face recognition process is also conducted in each component. When calculating the cosine similarity measure, (4.3) is replaced by the sum of four parts, that is, the setting method in the [27] is used.
- **RIPG-pure** [36]: The setting is the same as RIPG-full, except that only the  $\mathbf{X}_R$ ,  $\mathbf{X}_G$ , and  $\mathbf{X}_B$  are considered.
- **QPCA-full** [38]: The quaternion principal component analysis (QPCA) method for color face recognition, which encodes  $\mathbf{X}_{av}$  as the real part of the quaternion matrix  $\ddot{\mathbf{X}}$ .
- **QPCA-pure** [38]: The same as its original setting, i.e., let the real part of the quaternion matrix  $\ddot{\mathbf{X}}$  be a zero matrix.

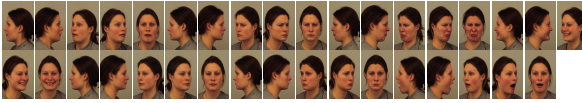
**Remark 6.** The purpose of choosing the above comparison methods is as follows: Comparing RBIPG with QIPG mainly aims to demonstrate the superiority of our model, NRBMF, after overcoming the model drawbacks of QNQMf (as discussed in Remark 1 and Remark 2). Comparing RBIPG with RIPG aims to highlight the superiority of the RB matrix over the real matrix in representing color images, as it treats the color channels as an integrated whole, fully utilizing and preserving the potential relationships between color channels. While QPCA is a representative quaternion-based color face recognition method in recent years.

### A. Color Face Recognition for AR Database [39]

In this experiment, we utilize a widely used subset of the AR database, consisting of 50 men and 50 women [40]. Each subject has 26 images captured during two distinct sessions (Session 1 and Session 2), encompassing varied lighting conditions, expressions, and occlusion (sunglasses or scarf). Figure 2(a) displays samples of one subject.



(a) Samples of one subject from AR database.



(b) Samples of one subject from KDEF database.

Fig. 2: Some samples of the used color face database.

We set up the experiments in the following two scenarios:

- (a) We exclude all faces with occlusion, such as sunglasses or scarves, using the remaining 14 face images per subject as samples. We randomly select 7 faces to construct the training set, and the remaining faces constitute the test set. All the color faces are resized to a spatial resolution of  $80 \times 60$ .
- (b) We retain all faces with occlusion, such as sunglasses or scarves, using all 26 face images per subject as samples. We select the 14 faces from Session 1 to construct the training set, and the 14 faces from Session 2 constitute the test set. All the color faces are resized to a spatial resolution of  $80 \times 60$ .

### B. Color Face Recognition for KDEF Database [41]

In this experiment, we utilize another commonly used face database, called the Karolinska Directed Emotional Faces (KDEF). It consists of a total of 4900 faces showing 70 individuals (35 women and 35 men) displaying 7 different emotional expressions (Angry, Fearful, Disgusted, Sad, Happy, Surprised, and Neutral). Each expression is viewed from 5 different angles and was recorded twice (the A and B series). Figure 2(b) displays samples of one subject. We set up the experiments in the following two scenarios:

- (c) We randomly select 17 faces from the A serie to construct the training set, and the remaining 18

TABLE III: The recognition accuracy of different methods under experiment V-A.

$l$	$l = 10$	$l = 20$	$l = 30$	$l = 40$	$l = 50$
Methods:	Scenario (a)				
RBIPG-full	<b>54.43%</b>	<b>72.00%</b>	<b>74.29%</b>	<b>79.20%</b>	<b>83.57%</b>
RBIPG-pure	51.43%	66.71%	72.86%	77.43%	81.57%
QIPG-full	49.57%	61.57%	73.14%	74.43%	78.57%
QIPG-pure	50.29%	64.29%	73.43%	78.14%	81.00%
RIPG-full	52.71%	66.00%	73.00%	76.00%	79.57%
RIPG-pure	53.43%	66.29%	73.14%	75.71%	78.86%
QPCA-full	51.57%	59.57%	64.14%	66.71%	67.71%
QPCA-pure	52.43%	60.71%	64.71%	67.29%	68.29%
Methods:	Scenario (b)				
RBIPG-full	<b>42.92%</b>	<b>55.08%</b>	<b>59.85%</b>	<b>64.31%</b>	<b>66.23%</b>
RBIPG-pure	40.54%	53.38%	56.85%	60.12%	63.46%
QIPG-full	35.23%	48.92%	55.46%	61.38%	63.38%
QIPG-pure	39.38%	51.69%	56.31%	62.15%	64.54%
RIPG-full	42.23%	52.15%	57.23%	62.23%	64.46%
RIPG-pure	41.92%	52.69%	57.31%	62.85%	64.38%
QPCA-full	40.92%	48.85%	52.85%	55.00%	56.38%
QPCA-pure	41.69%	50.00%	53.38%	55.54%	57.08%

faces constitute the test set. All color faces are resized to a spatial resolution of  $80 \times 100$ .

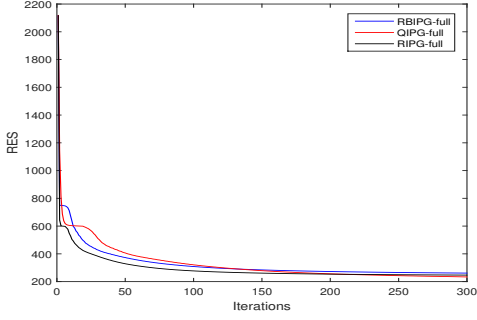
- (d) We randomly select 12 faces from the B serie to construct the training set, and the remaining 23 faces constitute the test set. All color faces are resized to a spatial resolution of  $80 \times 100$ .

TABLE IV: The recognition accuracy of different methods under experiment V-B.

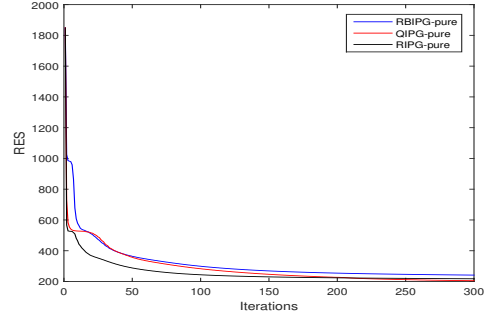
$l$	$l = 5$	$l = 10$	$l = 15$	$l = 20$	$l = 25$
Methods:	Scenario (c)				
RBIPG-full	<b>77.38%</b>	<b>90.71%</b>	<b>92.38%</b>	<b>93.81%</b>	<b>93.89%</b>
RBIPG-pure	76.59%	85.08%	90.71%	91.75%	92.46%
QIPG-full	67.06%	87.46%	89.13%	91.03%	92.86%
QIPG-pure	67.94%	87.86%	90.79%	92.14%	93.10%
RIPG-full	71.35%	88.33%	90.79%	91.90%	92.94%
RIPG-pure	72.54%	88.17%	90.79%	91.59%	92.70%
QPCA-full	68.65%	84.44%	89.84%	91.19%	92.54%
QPCA-pure	69.92%	85.40%	90.40%	91.59%	92.78%
Methods:	Scenario (d)				
RBIPG-full	<b>69.81%</b>	<b>82.86%</b>	<b>84.29%</b>	<b>86.40%</b>	<b>88.70%</b>
RBIPG-pure	63.73%	79.13%	82.11%	85.34%	87.20%
QIPG-full	57.20%	76.96%	80.81%	83.66%	86.46%
QIPG-pure	57.02%	78.51%	81.86%	84.41%	87.27%
RIPG-full	61.86%	78.57%	82.67%	85.34%	86.89%
RIPG-pure	63.85%	78.57%	82.24%	85.59%	87.33%
QPCA-full	60.56%	76.40%	82.24%	84.60%	85.65%
QPCA-pure	62.05%	77.27%	82.55%	85.16%	86.27%

Figure 3 presents the reconstruction residual (RES) versus iterations for RBIPG, QIPG, and RIPG under





(a) The ‘full’ case for different methods,  $l = 50$



(b) The ‘pure’ case for different methods,  $l = 50$

Fig. 3: RES versus iterations for different methods under experiment V-A, Scenario (a).

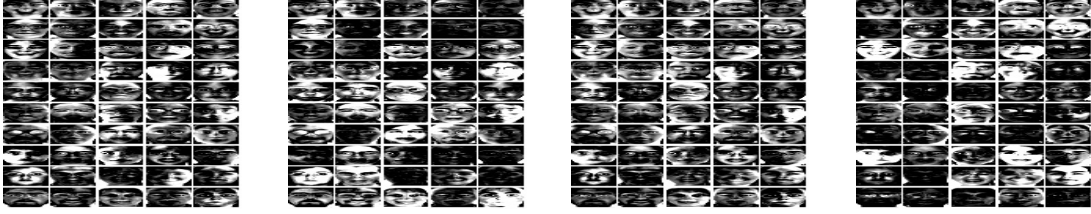
experiment V-A, Scenario (a). For RBIPG,  $RES = \|\tilde{\mathbf{X}} - \tilde{\mathbf{W}}\tilde{\mathbf{H}}\|_F$ ; for QIPG,  $RES = \|\tilde{\mathbf{X}} - \tilde{\mathbf{W}}\tilde{\mathbf{H}}\|_F$ ; for RIPG-full,  $RES = (\sum_{s=0}^3 \|\mathbf{X}_s - \mathbf{W}_s\mathbf{H}_s\|_F^2)^{1/2}$ ; and for RIPG-pure,  $RES = (\sum_{s=1}^3 \|\mathbf{X}_s - \mathbf{W}_s\mathbf{H}_s\|_F^2)^{1/2}$ . From Figure 3, we can observe that these algorithms all tend to converge within 300 iterations. After convergence, the sizes of the RES are relatively close, with the RES of RBIPG being slightly higher than those of QIPG and RIPG. We speculate that this is primarily due to the more restrictive nature of our model NRBMF, as it not only enforces non-negativity constraints but also requires the  $i$  and  $k$  parts of  $\tilde{\mathbf{H}}$  to be zero. However, due to the deficiencies of the QNQMf model and the fact that the NMF model does not consider the potential relationships between color channels, the slightly lower RES value does not imply that they can achieve better basis and encoding coefficient matrices.

Figure 4 and Figure 5 respectively show the basis matrices of RBIPG, QIPG, and RIPG under the ‘full’ and ‘pure’ settings in Scenario (a) of experiment V-A with  $l = 50$ . Figure 6 shows the encoding coefficients of RBIPG, QIPG, and RIPG under the ‘full’ setting in Scenario (a) of experiment V-A with  $l = 50$ . Results for the ‘pure’ case can be found in the Supplementary Materials. Figures 7 demonstrates the sparsity of the encoding coefficients (SEC) obtained by RBIPG, QIPG, and RIPG under the ‘full’ setting. Results for the ‘pure’ case can be found in the Supplementary Materials. SEC is defined as (21). Tables III and IV present the face recognition accuracy of different methods in experiments V-A and V-B. From these experimental results, we mainly observe the following points:

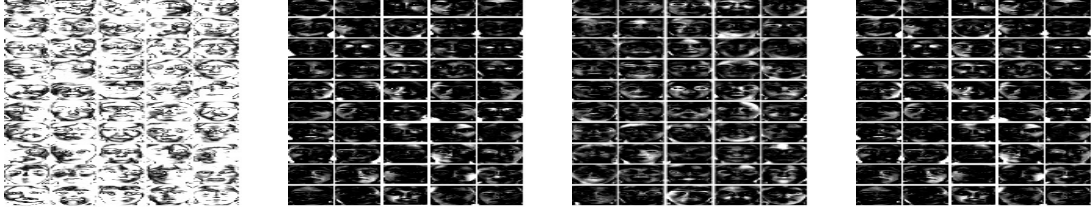
- 1) Comparing the results of RBIPG-full and RBIPG-pure, we notice that in Figure 5(a), a significant number of features in parts  $\text{Re}(\tilde{\mathbf{W}})$  and  $\text{Im}_j(\tilde{\mathbf{W}})$

have disappeared compared to Figure 4(a). This observation is consistent with the analysis presented in Remark 4, indicating that our model is more suitable for the ‘full’ setting. The comparison of face recognition accuracy between RBIPG-full and RBIPG-pure in Tables III and IV also supports this conclusion. However, for QIPG, RIPG, and QPCA, the face recognition accuracy obtained with the ‘full’ setting is not higher than that obtained with the ‘pure’ setting. This is quite natural, as the introduction of  $\mathbf{X}_{av}$  does not add additional feature information; instead, it makes the information slightly redundant, which may lead to a decrease in the recognition accuracy of these methods.

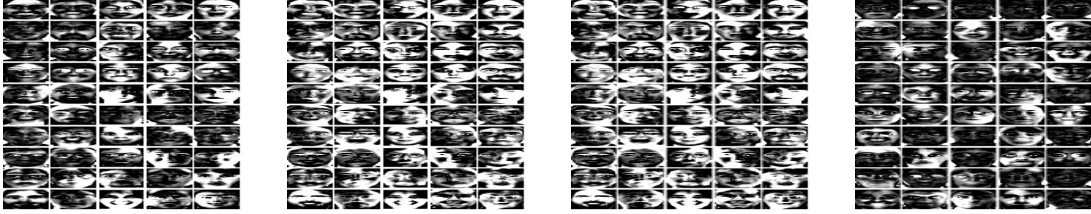
- 2) Following the characteristics of NMF, the basis images obtained by these methods should exhibit a certain degree of sparsity. Figures 4 and 5 show that, compared to RBIPG and RIPG, the sparsity of the basis images obtained by QIPG is highly unbalanced. Specifically, the  $\text{Re}(\tilde{\mathbf{W}})$  part of  $\tilde{\mathbf{W}}$  obtained by QIPG is not sparse at all (we use  $\text{abs}(\text{Re}(\tilde{\mathbf{W}}))$  because  $\text{Re}(\tilde{\mathbf{W}})$  contains negative numbers), even though parts  $\text{Im}_i(\tilde{\mathbf{W}})$ ,  $\text{Im}_j(\tilde{\mathbf{W}})$ , and  $\text{Im}_k(\tilde{\mathbf{W}})$  appear to be very sparse. Such inexplicable result may be due to the inherent shortcomings of the QNQMf model. In addition, it can be observed from Figures 4 and 5 that the basis images obtained by our RBIPG method are slightly sparser compared to those obtained by the RIPG method. For Figures 4 and 5, by simply calculating the proportion of zero elements (*i.e.*, sparsity) in all the basis images obtained by each method, we



(a) Basis images computed by RBIPG-full; From left to right are the  $\text{Re}(\ddot{\mathbf{W}})$ ,  $\text{Im}_i(\ddot{\mathbf{W}})$ ,  $\text{Im}_j(\ddot{\mathbf{W}})$ , and  $\text{Im}_k(\ddot{\mathbf{W}})$ .

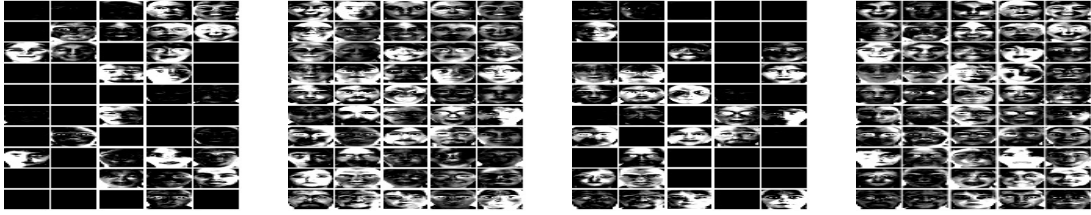


(b) Basis images computed by QIPG-full; From left to right are the  $\text{abs}(\text{Re}(\dot{\mathbf{W}}))$ ,  $\text{Im}_i(\dot{\mathbf{W}})$ ,  $\text{Im}_j(\dot{\mathbf{W}})$ , and  $\text{Im}_k(\dot{\mathbf{W}})$ .

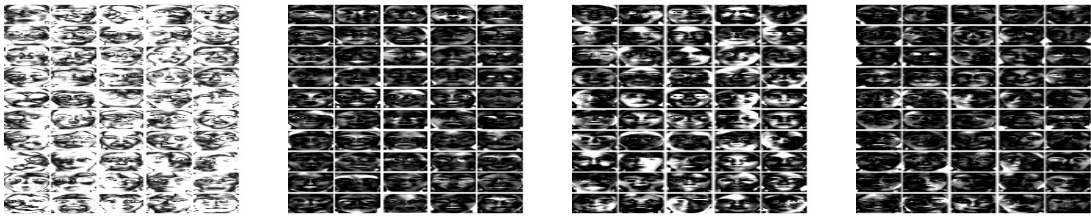


(c) Basis images computed by RIPG-full; From left to right are the  $\mathbf{W}_{av}$ ,  $\mathbf{W}_R$ ,  $\mathbf{W}_G$ , and  $\mathbf{W}_B$ .

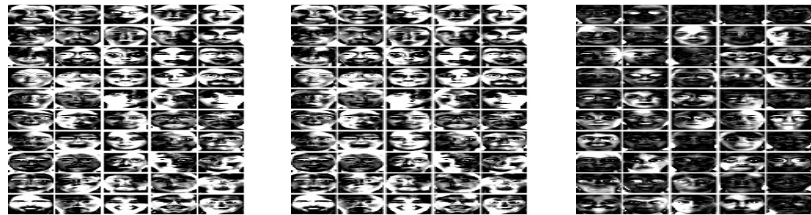
Fig. 4: Basis images of different methods with the ‘full’ case under Scenario (a) of experiment V-A with  $l = 50$ .



(a) Basis images computed by RBIPG-pure; From left to right are the  $\text{Re}(\ddot{\mathbf{W}})$ ,  $\text{Im}_i(\ddot{\mathbf{W}})$ ,  $\text{Im}_j(\ddot{\mathbf{W}})$ , and  $\text{Im}_k(\ddot{\mathbf{W}})$ .

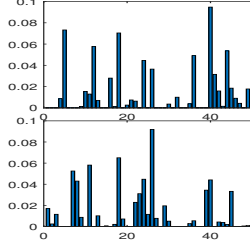
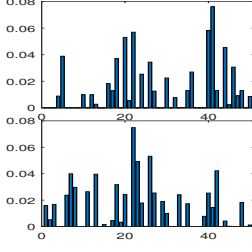


(b) Basis images computed by QIPG-pure; From left to right are the  $\text{abs}(\text{Re}(\dot{\mathbf{W}}))$ ,  $\text{Im}_i(\dot{\mathbf{W}})$ ,  $\text{Im}_j(\dot{\mathbf{W}})$ , and  $\text{Im}_k(\dot{\mathbf{W}})$ .

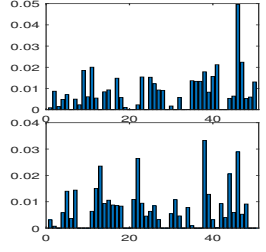
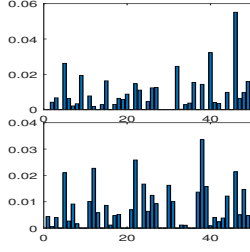
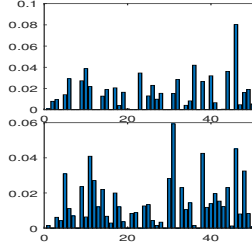
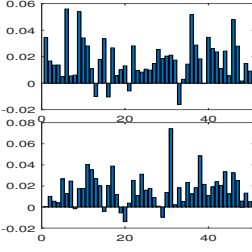


(c) Basis images computed by RIPG-pure; From left to right are the  $\mathbf{W}_R$ ,  $\mathbf{W}_G$ , and  $\mathbf{W}_B$ .

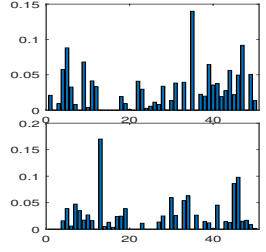
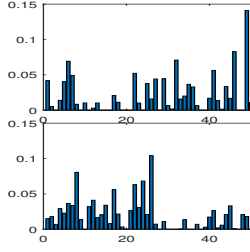
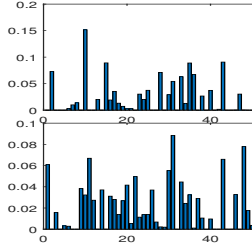
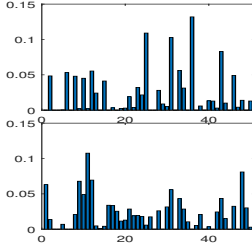
Fig. 5: Basis images of different methods with the ‘pure’ case under Scenario (a) of experiment V-A with  $l = 50$ .



(a) Encoding coefficients computed by RBIPG-full; From left to right are the 10th column (first row) and the 100th column (second row) of  $\text{Re}(\mathbf{\tilde{H}})$  and  $\text{Im}_j(\mathbf{\tilde{H}})$ .



(b) Encoding coefficients computed by QIPG-full; From left to right are the 10th column (first row) and the 100th column (second row) of  $\text{Re}(\mathbf{\tilde{H}})$ ,  $\text{Im}_i(\mathbf{\tilde{H}})$ ,  $\text{Im}_j(\mathbf{\tilde{H}})$ , and  $\text{Im}_k(\mathbf{\tilde{H}})$ .



(c) Encoding coefficients computed by RIPG-full; From left to right are the 10th column (first row) and the 100th column (second row) of  $\mathbf{H}_{av}$ ,  $\mathbf{H}_R$ ,  $\mathbf{H}_G$ , and  $\mathbf{H}_B$ .

Fig. 6: The encoding coefficients of RBIPG-full (a), QIPG-full (b), and RIPG-full (c) under Scenario (a) of experiment V-A with  $l = 50$ .

get: RBIPG-full<sup>1</sup> at 33.86%, QIPG-full at 28.89%, RIPG-full at 29.55%, QIPG-pure at 20.85%, and RIPG-pure at 29.42%. Thus, our RBIPG method can obtain relatively sparser basis images<sup>2</sup>.

- 3) The encoding coefficients reflect the weights of the basis images, and the intrinsic features between different faces should be distinct. Theoretically, this would result in the encoding coefficients exhibiting a certain degree of sparsity. In other words, if the encoding coefficients do not show significant sparsity, then the decomposition model

<sup>1</sup>Although the basis images obtained by RBIPG-pure are noticeably sparser, based on point 1) and the analysis in Remark 4, we primarily focus on the results of RBIPG-full.

<sup>2</sup>For other values of  $l$  and data, we can obtain the same conclusion.

is not sufficiently reasonable. From Figure 6, it can be observed that the encoding coefficients obtained by RBIPG are sparser than those obtained by QIPG and RIPG. This conclusion is also clearly supported by the quantitative comparison in Figure 7. Furthermore, from Figure 6(b), it can be observed that the  $\text{Re}(\mathbf{\tilde{H}})$  part of the encoding coefficients obtained by QIPG contains negative values, which is unreasonable. This issue is mainly caused by the inherent drawbacks in the design of the QNQMFM model.

- 4) From Tables III and IV, it is clear that our RBIPG-full method has an advantage in color face recognition, which is consistent with our previous analysis

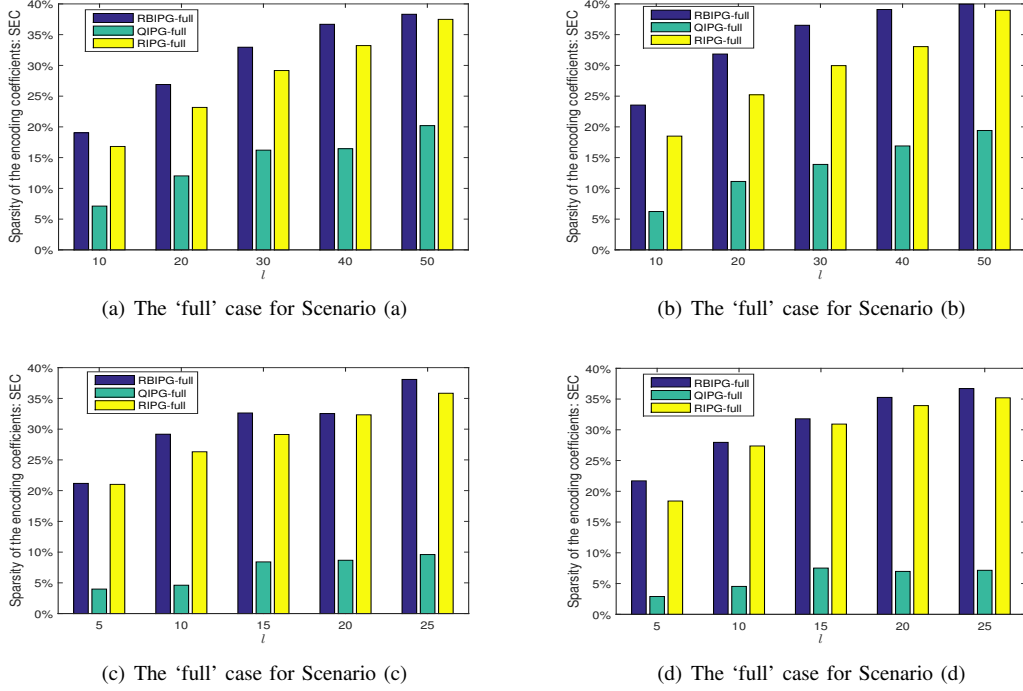


Fig. 7: Comparison of SEC with different values of  $l$  under experiments V-A and V-B.

$$\begin{aligned}
\text{SEC} &= \frac{\text{num}_1(\text{Re}(\ddot{\mathbf{H}})) + \text{num}_1(\text{Im}_j(\ddot{\mathbf{H}}))}{\text{num}(\text{Re}(\ddot{\mathbf{H}})) + \text{num}(\text{Im}_j(\ddot{\mathbf{H}}))} 100\%, \text{ for RBIPG;} \\
\text{SEC} &= \frac{\text{num}_1(\text{abs}(\text{Re}(\dot{\mathbf{H}}))) + \text{num}_1(\text{Im}_i(\dot{\mathbf{H}})) + \text{num}_1(\text{Im}_j(\dot{\mathbf{H}})) + \text{num}_1(\text{Im}_k(\dot{\mathbf{H}}))}{\text{num}(\text{Re}(\dot{\mathbf{H}})) + \text{num}(\text{Im}_i(\dot{\mathbf{H}})) + \text{num}(\text{Im}_j(\dot{\mathbf{H}})) + \text{num}(\text{Im}_k(\dot{\mathbf{H}}))} 100\%, \text{ for QIPG;} \\
\text{SEC} &= \frac{\text{num}_1(\mathbf{H}_{av}) + \text{num}_1(\mathbf{H}_R) + \text{num}_1(\mathbf{H}_G) + \text{num}_1(\mathbf{H}_B)}{\text{num}(\mathbf{H}_{av}) + \text{num}(\mathbf{H}_R) + \text{num}(\mathbf{H}_G) + \text{num}(\mathbf{H}_B)} 100\%, \text{ for RIPG-full;} \\
\text{SEC} &= \frac{\text{num}_1(\mathbf{H}_R) + \text{num}_1(\mathbf{H}_G) + \text{num}_1(\mathbf{H}_B)}{\text{num}(\mathbf{H}_R) + \text{num}(\mathbf{H}_G) + \text{num}(\mathbf{H}_B)} 100\%, \text{ for RIPG-pure,}
\end{aligned} \tag{21}$$

where  $\text{num}(\mathbf{A})$  returns the total number of elements in  $\mathbf{A}$ , while  $\text{num}_1(\mathbf{A})$  returns the number of elements in  $\mathbf{A}$  that are less than  $1e^{-5}$ .

and expectations.

## VI. CONCLUSIONS

In the paper, we introduced a concept of the non-negative reduced biquaternion (RB) matrix and proposed a non-negative RB matrix factorization (NRBMF) model based on the multiplication properties of RB. The proposed NRBMF model effectively addressed the two limitations of the recently introduced quasi non-negative quaternion matrix factorization (QNQMF) model, thereby providing a novel theoretical tool for color image processing. A method for computing the gradient of a real-valued function with RB matrices as

variables was proposed, and an efficient RB projected gradient algorithm for the optimization problem of the NRBMF model was developed. Additionally, a convergence analysis of the algorithm was provided. Furthermore, the effectiveness and superiority of the proposed model were verified through numerical experiments on color face recognition. These initial results are highly promising and set the stage for future work on both the theoretical and methodological aspects of NRBMF.

In future work, we may consider further improving the NRBMF model, such as developing a sparse NRBMF and researching error measures more suitable for NRBMF (other than the Least Squares criterion) to

better apply it to color face recognition. Additionally, we aim to apply this model or its improved versions to other color image processing tasks, such as color image denoising and color image restoration.

## REFERENCES

- [1] D. D. Lee and H. S. Seung, "Learning the parts of objects by non-negative matrix factorization," *nature*, vol. 401, no. 6755, pp. 788–791, 1999.
- [2] N. Gillis, "The why and how of nonnegative matrix factorization," *Regularization, optimization, kernels, and support vector machines*, vol. 12, no. 257, pp. 257–291, 2014.
- [3] B. Ren, L. Pueyo, G. B. Zhu, J. Debes, and G. Duchêne, "Non-negative matrix factorization: robust extraction of extended structures," *The Astrophysical Journal*, vol. 852, no. 2, p. 104, 2018.
- [4] D. Guillet and J. Vitria, "Non-negative matrix factorization for face recognition," in *Catalonian Conference on Artificial Intelligence*. Springer, 2002, pp. 336–344.
- [5] Y. Wang, Y. Jia, C. Hu, and M. Turk, "Non-negative matrix factorization framework for face recognition," *International Journal of Pattern Recognition and Artificial Intelligence*, vol. 19, no. 04, pp. 495–511, 2005.
- [6] F. Nikan and H. Hassanpour, "Face recognition using non-negative matrix factorization with a single sample per person in a large database," *Multimedia Tools and Applications*, vol. 79, no. 37, pp. 28 265–28 276, 2020.
- [7] W.-S. Chen, X. Ge, and B. Pan, "A novel general kernel-based non-negative matrix factorisation approach for face recognition," *Connection Science*, vol. 34, no. 1, pp. 785–810, 2022.
- [8] A. Yip and P. Sinha, "Role of color in face recognition," 2001.
- [9] L. Torres, J.-Y. Reutter, and L. Lorente, "The importance of the color information in face recognition," in *Proceedings 1999 International Conference on Image Processing (Cat. 99CH36348)*, vol. 3. IEEE, 1999, pp. 627–631.
- [10] X. Xiang, J. Yang, and Q. Chen, "Color face recognition by pca-like approach," *Neurocomputing*, vol. 152, pp. 231–235, 2015.
- [11] C. Zou, K. I. Kou, and Y. Wang, "Quaternion collaborative and sparse representation with application to color face recognition," *IEEE Transactions on image processing*, vol. 25, no. 7, pp. 3287–3302, 2016.
- [12] S.-T. Ling, Y.-D. Li, B. Yang, and Z.-G. Jia, "Joint diagonalization for a pair of hermitian quaternion matrices and applications to color face recognition," *Signal Processing*, vol. 198, p. 108560, 2022.
- [13] M. Rajapakse, J. Tan, and J. Rajapakse, "Color channel encoding with nmf for face recognition," in *2004 International Conference on Image Processing, 2004. ICIP'04.*, vol. 3. IEEE, 2004, pp. 2007–2010.
- [14] X. Bai and C. Wang, "Improved nmf algorithm based color face recognition," in *2010 8th World Congress on Intelligent Control and Automation*. IEEE, 2010, pp. 6366–6370.
- [15] W. R. Hamilton, *Elements of quaternions*. London: Longmans, Green, & Company, 1866.
- [16] C. Segre, "The real representations of complex elements and extension to bicomplex systems," *Math. Ann.*, vol. 40, pp. 413–467, 1892.
- [17] S.-C. Pei, J.-H. Chang, and J.-J. Ding, "Commutative reduced biquaternions and their fourier transform for signal and image processing applications," *IEEE Transactions on Signal Processing*, vol. 52, no. 7, pp. 2012–2031, 2004.
- [18] J. Miao and K. I. Kou, "Quaternion-based bilinear factor matrix norm minimization for color image inpainting," *IEEE Transactions on Signal Processing*, vol. 68, pp. 5617–5631, 2020.
- [19] —, "Color image recovery using low-rank quaternion matrix completion algorithm," *IEEE Transactions on Image Processing*, vol. 31, pp. 190–201, 2021.
- [20] G. Song, W. Ding, and M. K. Ng, "Low rank pure quaternion approximation for pure quaternion matrices," *SIAM Journal on Matrix Analysis and Applications*, vol. 42, no. 1, pp. 58–82, 2021.
- [21] Y. Yu, Y. Zhang, and S. Yuan, "Quaternion-based weighted nuclear norm minimization for color image denoising," *Neuro-computing*, vol. 332, pp. 283–297, 2019.
- [22] J. Han, K. I. Kou, and J. Miao, "Quaternion-based dynamic mode decomposition for background modeling in color videos," *Computer Vision and Image Understanding*, vol. 224, p. 103560, 2022.
- [23] M. T. El-Melegy and A. T. Kamal, "Color image processing using reduced biquaternions with application to face recognition in a pca framework," in *Proceedings of the IEEE International Conference on Computer Vision Workshops*, 2017, pp. 3039–3046.
- [24] S. Gai, "Theory of reduced biquaternion sparse representation and its applications," *Expert Systems with Applications*, vol. 213, p. 119245, 2023.
- [25] Z. Guo, T. Jiang, G. Wang, and V. Vasil'ev, "Algebraic algorithms for eigen-problems of a reduced biquaternion matrix and applications," *Applied Mathematics and Computation*, vol. 463, p. 128358, 2024.
- [26] J. Flamant, S. Miron, and D. Brie, "Quaternion non-negative matrix factorization: Definition, uniqueness, and algorithm," *IEEE Transactions on Signal Processing*, vol. 68, pp. 1870–1883, 2020.
- [27] Y. Ke, C. Ma, Z. Jia, Y. Xie, and R. Liao, "Quasi non-negative quaternion matrix factorization with application to color face recognition," *Journal of Scientific Computing*, vol. 95, no. 2, p. 38, 2023.
- [28] H.-D. Schutte and J. Wenzel, "Hypercomplex numbers in digital signal processing," in *1990 IEEE International Symposium on Circuits and Systems (ISCAS)*. IEEE, 1990, pp. 1557–1560.
- [29] V. S. Dimitrov, T. Cooklev, and B. Donevsky, "On the multiplication of reduced biquaternions and applications," *Information processing letters*, vol. 43, no. 3, pp. 161–164, 1992.
- [30] S.-C. Pei, J.-H. Chang, J.-J. Ding, and M.-Y. Chen, "Eigenvalues and singular value decompositions of reduced biquaternion matrices," *IEEE Transactions on Circuits and Systems I: Regular Papers*, vol. 55, no. 9, pp. 2673–2685, 2008.
- [31] M. T. El-Melegy and A. T. Kamal, "Linear regression classification in the quaternion and reduced biquaternion domains," *IEEE Signal Processing Letters*, vol. 29, pp. 469–473, 2022.
- [32] C. M. Davenport, "A commutative hypercomplex algebra with associated function theory," 1996.
- [33] L. Qi, Z. Luo, Q.-W. Wang, and X. Zhang, "Quaternion matrix optimization: Motivation and analysis," *Journal of Optimization Theory and Applications*, vol. 193, no. 1, pp. 621–648, 2022.
- [34] Y. Chen, L. Qi, X. Zhang, and Y. Xu, "A low rank quaternion decomposition algorithm and its application in color image inpainting," *arXiv preprint arXiv:2009.12203*, 2020.
- [35] D. P. Bertsekas, "On the goldstein-levitin-polyak gradient projection method," *IEEE Transactions on automatic control*, vol. 21, no. 2, pp. 174–184, 1976.
- [36] C.-J. Lin, "Projected gradient methods for nonnegative matrix factorization," *Neural computation*, vol. 19, no. 10, pp. 2756–2779, 2007.
- [37] C.-J. Lin and J. Jorge, "Moré. newton's method for large-scale bound constrained problems," *SIAM Journal on Optimization*, vol. 9, no. 1100-1127, pp. 10–1137, 1999.
- [38] W. Liu, K. I. Kou, J. Miao, and Z. Cai, "Quaternion scalar and vector norm decomposition: Quaternion pca for color face recognition," *IEEE Transactions on Image Processing*, vol. 32, pp. 446–457, 2022.
- [39] A. Martinez and R. Benavente, "The ar face database, cvc," *Copyright of Informatica (03505596)*, 1998.
- [40] J. Wright, A. Y. Yang, A. Ganesh, S. S. Sastry, and Y. Ma, "Robust face recognition via sparse representation," *IEEE transactions on pattern analysis and machine intelligence*, vol. 31, no. 2, pp. 210–227, 2008.

- [41] D. Lundqvist, A. Flykt, and A. Öhman, “Karolinska directed emotional faces,” *PsycTESTS Dataset*, vol. 91, p. 630, 1998.